Static third-harmonic lines in widely variable fiber continuum generation

Haohua Tu, Youbo Zhao, Yuan Liu, and Stephen A. Boppart
Beckman Institute for Advanced Science and Technology, University of Illinois at Urbana-Champaign, Urbana, Illinois 61801, USA
(Received 28 September 2012; revised manuscript received 18 September 2013; published 13 January 2014)

An intriguing phenomenon of third-harmonic generation under fiber continuum generation is the emission of an anharmonic signal. One popular interpretation of this effect has developed into a general theory of fiber third-harmonic generation. Here we produce "static" third-harmonic lines dictated fully by fiber properties independent of pump parameters, in contrast to the signals of all known phase-matched nonlinear optical processes that vary dynamically with these parameters. We argue that the anharmonic signal is an illusion of the continuum generation, that it is in fact harmonic, and that this theory should be reevaluated.

DOI: 10.1103/PhysRevA.89.013813 PACS number(s): 42.65.Ky, 42.79.Nv, 42.81.Qb

In the phase-matching condition of bulk crystals corresponding to third-harmonic generation (THG), a given pump of optical frequency ω_p produces THG signal at exactly $3\omega_p$. This condition, when applied to a multimode waveguide with a length much longer than the coherence buildup length of the THG, can be written as

$$\Delta\beta = \beta^h(3\omega_p) - 3\beta(\omega_p) = 0 \ \text{(regular)}, \tag{1}$$

where β and β^h are modal propagation constants of the pump (fundamental mode) and signal, respectively. This equation reveals the momentum and energy conservations of interacting photons. It is thus rather surprising that anharmonic signal generation at ω_h ($\omega_h \neq 3\omega_p$) has been observed in long (>1 cm) multimode fibers during continuum generation [1,2]. One simple interpretation is to include the well-known Kerr-effect correction to the propagation constants Taylor expanded at ω_p, resulting in a generalized phase-matching condition of

$$\sum_{n=0}^{n=\infty} \frac{(\Delta\beta)_n}{n!}\Omega^n + 3\gamma P = 0 \ \text{(dynamic view)}, \tag{2}$$

where $\Omega = (\omega_h - 3\ \omega_p)$ (anharmonic shift) is the correction of the THG due to the Kerr-effect $3\gamma P$ at a nonlinear coefficient γ and a pump (peak) power P [3–5]. Dynamic anharmonic signal generation with a pump-dependent nonzero Ω is expected because the parallel treatment of four-wave mixing (FWM) (another four-photon $\chi^{(3)}$ process [5] similar to the THG) has successfully predicted the dynamic Stokes detuning Ω_s by the Kerr-effect correction using either the low-order or generalized phase-matching condition (Table I) [6,7]. This FWM has formed the basis of widely tunable fiber parametric amplifiers or oscillators [5]. The corresponding low-order (or weak-pump) THG phase-matching condition (Table I) has seemingly reproduced the anharmonic effect [2], while the underlying theory predicted the unusual effect of signal spectral narrowing [3]. Due to the dynamic nature of the signal, the above interpretation can be denoted as a *dynamic view*, which has been theoretically extended to explain other dynamic features of the signal, including spectral asymmetries [8] and large soliton-induced redshifts [9,10]. Currently, this view anchors the most general theory of fiber THG. As to the numerous reports of strictly harmonic signal generation (e.g., [11]), the theory asserts that the Kerr effect is negligible, and the generalized phase-matching condition of Eq. (2) is reduced to the regular one of Eq. (1).

There is, however, an alternative and incompatible interpretation of the anharmonic effect [1,12], termed as the *static view*, which treats the spectral positions of the signal as "static" properties dictated fully by fiber structure. The fundamental of a given signal ω_h is not attributed to ω_p (pump), but somewhat artificially to the continuum component of $\omega_h/3$ that differs from ω_p, yielding a phase-matching condition of

$$\beta^h(\omega_h) - 3\beta\left(\frac{\omega_h}{3}\right) = 0 \ \text{(static view)}. \tag{3}$$

This equation is deceptively similar to Eq. (1). However, it should be noted that the generalized phase-matching condition of the dynamic view cannot be reduced to Eq. (3) by simply neglecting the Kerr effect, because $\omega_h \neq 3\omega_p$. Thus, the seemingly "normal" static view is highly "radical," because its phase-matching condition has no pump dependence, a universal property of phase-matched nonlinear optical processes found not only in bulk materials but also in waveguides. Experimentally, the static view was supported by the prediction of signal wavelengths and modes from fiber structure [1,12]. However, this is ambiguous because similar simulations have made such prediction from the dynamic view [3,10,13]. The insensitivity of signal wavelength to the pump could be the definitive evidence [12], except for the claims that the dynamic view could lead to the same conclusion [3,13]. These factors may have contributed to the lower popularity of the static view. Here we present unambiguous evidence that favors the static view over the dynamic view, and draw the analogy of observed THG lines to the "static" atomic absorption lines present in a continuum irradiation spectrum.

In our experiments, multimode photonic crystal fibers are employed (Table II), with each having the same cross-sectional image (Fig. 1, inset A), but with different core sizes. A tunable Ti:sapphire laser (690–1020 nm, ~100 fs, 80 MHz) is used to pump these fibers for widely variable continuum generation. An aspheric lens enables 40%–70% coupling of the laser to the fiber fundamental mode, with variable coupling power by varying the incident laser power. The fiber output is collimated by an off-axis parabolic aluminum mirror, and then refocused by another similar mirror onto the entrance fiber of an ultraviolet spectrometer (spectral window: 250–385 nm, resolution: 0.07 nm) to detect the THG, or that of a near-infrared optical spectrum analyzer (set spectral window: 750–1155 nm) to locate its fundamental in the continuum.

TABLE I. Phase-matching conditions for fiber THG and FWM.

Condition	THG (intermodal)	FWM (single mode)
Regular	$\Delta\beta = \beta^h(3\omega_p) - 3\beta(\omega_p) = 0$	$\Delta\beta = \beta(\omega_p + \Omega_s) + \beta(\omega_p - \Omega_s) - 2\beta(\omega_p) = 0$
Dynamic view (generalized)	$(\Delta\beta)_0 + (\Delta\beta)_1\Omega + (\Delta\beta)_2\Omega^2/2! + \cdots + 3\gamma P = 0$	$\beta_2\Omega_s^2/2! + \beta_4\Omega_s^4/4! + \beta_6\Omega_s^6 + \cdots + 2\gamma P = 0$
Dynamic view (low order)	$(\Delta\beta)_0 + (\Delta\beta)_1\Omega + 3\gamma P = 0$	$\beta_2\Omega_s^2/2! + \beta_4\Omega_s^4/4! + 2\gamma P = 0$
Dynamic view (weak pump)	$(\Delta\beta)_0 + (\Delta\beta)_1\Omega = 0$	$\beta_2\Omega_s^2/2! + \beta_4\Omega_s^4/4! = 0$
Static view	$\beta^h(\omega_h) - 3\beta(\omega_h/3) = 0$	No report

Simultaneously observed fiber output spectra in the two windows at a variety of conditions (fiber type and length, pump wavelength, and coupling power) are compared in Figs. 1(a)–1(g). At low coupling power with minimum continuum generation, a THG line of 302.6 nm is generated in the fiber NL-2.0-735 when the pump is tuned to its fundamental of 302.6×3 nm [Fig. 1(c)]. However, if the pump is detuned to 975 nm, no corresponding THG emission of 325 nm is observed. Rather, another line of 302.6 nm emerges when the blue edge of the continuum (dispersive wave) extends across 302.6×3 nm [Fig. 1(b)], with a thresholdlike dependence of emission intensity on the coupling power. The line stays at 302.6 ± 0.1 nm at higher coupling powers when the continuum extends beyond 302.6×3 nm (not shown). Similarly, if the pump is detuned to 805 nm, a third line of 302.6 nm emerges when the red edge of the continuum (soliton) extends across 302.6×3 nm [Fig. 1(a)], with similar threshold behavior and wavelength stability. The three lines reveal nearly identical symmetric spectra (Fig. 1, inset B), indicating the THG nature of the 302.6-nm lines in the two continuum cases, even though the signal can be generated far away from $3\omega_p$ with a large anharmonic blueshift Ω [green arrow, Fig. 1(b)].

The dynamic view of this convergence would require a delicate combination of the pump wavelength and coupling power (Kerr effect) to target the 302.6 nm [3,9,10,13], which is in contradiction with the observed wavelength stability against the coupling power. In contrast, the static view of this phenomenon simply attributes the emergence of the 302.6-nm (ω_h) THG lines to the presence of their fundamentals 302.6×3 nm ($\omega_h/3$) in the continuum, regardless of the pump wavelength and coupling power. We have confirmed the $\omega_h - \omega_h/3$ coincidence (static view) in a wide range of continuum generation. Note that this conclusion is also valid for the 331.1- and 353.4-nm THG lines that dominate the ultraviolet spectra of the fibers NL-2.3-790 and NL-2.6-825, respectively [Figs. 1(d)–1(g)], and for the weak THG lines [blue arrows, Figs. 1(a), 1(d), and 1(f)] that accompany the dominant THG lines. Thus, the anharmonic signal is an illusion of the continuum generation, and is indeed harmonic if the fundamental is accurately located. This may explain why anharmonic signal generation has not been reported in the absence of continuum generation. Without the widely variable continuum generation [Figs. 1(a)–1(g)], prior studies supporting the static view [1,12] were unable to accurately locate the fundamental within the generated broadband continuum, and to shift the dynamic view toward the static one.

The dynamic view of the observed anharmonic blueshifts [green arrows, Figs. 1(b) and 1(e)] necessitates a large Kerr effect (coupling power effect) on the signal wavelength [3–5]. This is tested for the 331.1-nm line under direct pump stimulation [Figs. 2(a) and 2(b)], where the strongest THG is observed, and therefore the largest Kerr effect is expected. At low coupling powers, the intensity of this line follows an expected third-order dependence on the coupling power [Fig. 2(a)]. At the highest coupling power, which is limited by fiber optical damage, this line attains an average power of 0.15 mW, or a THG conversion efficiency of 0.2%. In a dynamic range of signal intensity over three orders of magnitude [Fig. 2(a)], the central wavelength and symmetric spectrum of the signal remain "static" [Fig. 2(b), inset]. No indication of the Kerr effect is found, even though the pump undergoes dramatic continuum transformation [Fig. 2(b)]. The absence of this Kerr effect before optical damage has been confirmed in other fibers, echoing the same conclusion from an independent study [11]. Prior studies supporting the static view [1,12] did not rule out the Kerr effect unambiguously, because of the low signal-to-noise ratio [1] or the coarse spectral resolution of intrinsically broad signal spectra [12] (for the reason that will be clarified below).

The observed signal spectrum is not only independent of the pump wavelength and coupling power, but also independent of pump polarization, indicating little influence from fiber birefringence. This complete deprivation of pump dependence is the hallmark of the static view. To simulate plausible THG wavelengths according to this view, the cross section of NL-2.3-790 is treated as an air-cladded hexagon strand of silica (Fig. 1, inset A) having a zero-dispersion wavelength (ZDW) of 790 nm. With no adjustable parameter, the edge

TABLE II. Intermodal third-harmonic generation in mode 32 from commercial photonic crystal fibers (NKT Photonics, Denmark).

Fiber type-core size-ZDW (nm)	NL-2.0-735	NL-2.0-745	NL-2.3-790	NL-2.4-800	NL-2.6-825
Hexagon edge (μm)	0.933	0.966	1.112	1.168	1.292
Signal λ ($\pm$0.1 nm) (obs.)	302.6	307.1	331.1	339.5	353.4
Signal λ (nm) (calc.)	302.2	307.8	331.5	340.4	359.9
FWHM ($\pm$0.04 nm) (obs.)	0.24	0.29	0.45	0.49	0.55
Differential slope (10^{-4} nm^{-1})	5.07	4.79	3.70	3.38	2.82

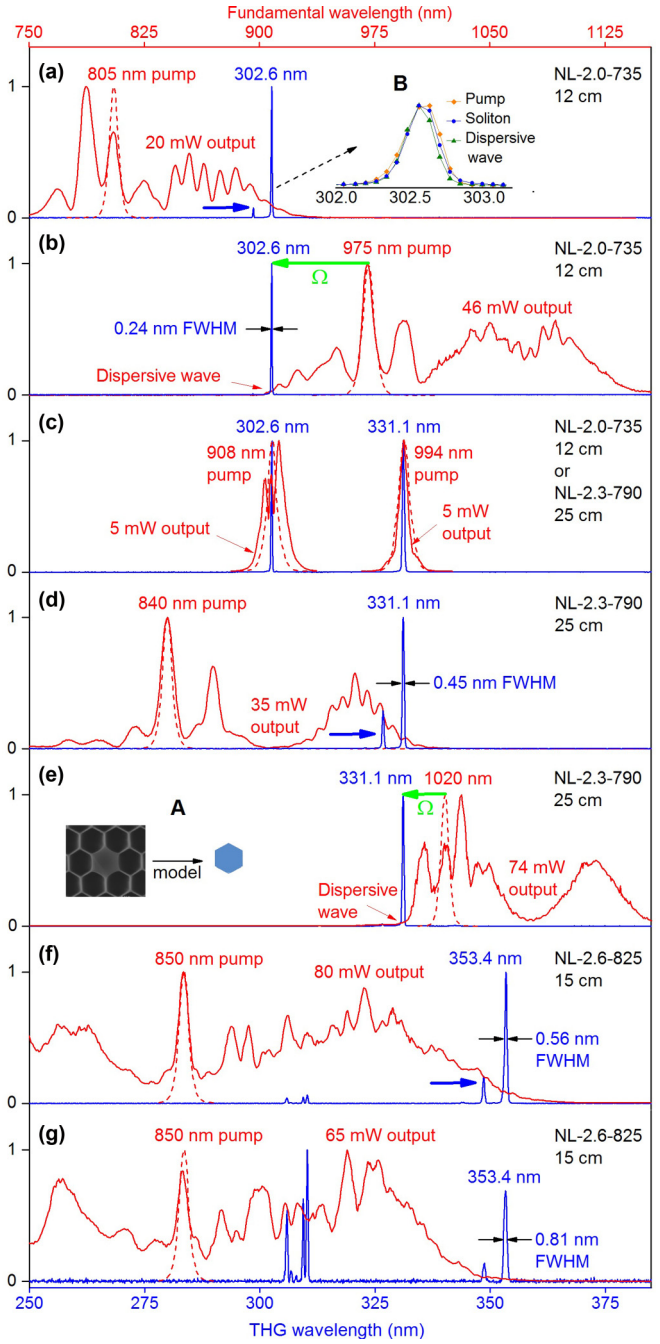

FIG. 1. (Color online) Comparison of simultaneously observed fiber output spectra in the ultraviolet window (blue curves, bottom scale) and the NIR window (red curves, top scale) at various conditions of pump spectrum (broken red curves, top scale), fiber type and length, and coupling power. Inset A: common cross-sectional image of the fibers and simplified fiber cross section for modeling. Inset B: comparison of THG spectra stimulated by pump itself, soliton, and dispersive wave for fiber NL-2.0-735.

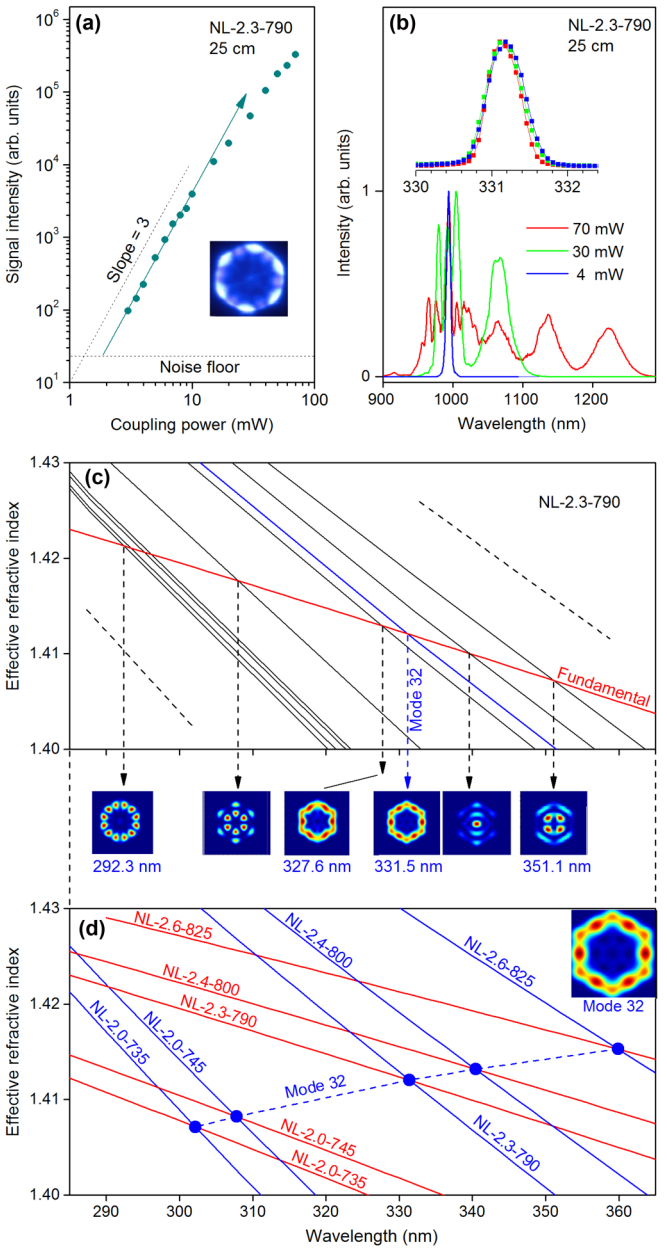

FIG. 2. (Color online) Observed properties of THG produced in mode 32. (a) THG intensity of fiber NL-2.3-790 as a function of coupling power at a fixed pump wavelength of 994 nm; inset: observed ultraviolet intensity pattern of collimated fiber output. (b) Corresponding continuum spectrum and THG spectrum (inset) at three coupling powers. (c) Intersections of effective index curves of higher-order modes (solid black or blue curves) with frequency-tripled effective index curve of fundamental mode (red curve) produce several phase-matched wavelengths (broken arrows) for fiber NL-2.3-790, with near-field intensity patterns of corresponding higher-order modes (insets). (d) Intersections of effective index curves (blue curves) of mode 32 (inset) with frequency-tripled effective index curve of fundamental mode (red curves) produce phase-matched wavelengths for five fibers (blue dots).

length of the hexagon can be derived (Table II) and the mode dispersion profiles of the silica strand subsequently calculated by a fully vectorial mode solver [Fig. 2(c)] [12]. Note that the effective index (n_{eff}) curve of the fundamental mode undergoes a $\omega \rightarrow 3\omega$ transformation [Fig. 2(c), red curve] to intersect those of high-order modes, giving rise to a few phase-matched wavelengths within the detectable ultraviolet window [Fig. 2(c), arrows]. The 32nd mode of the fiber, i.e., the spatial mode with the 32nd highest effective

refractive index among all guiding modes of the fiber [14], has a calculated phase-matched wavelength of 331.5 nm, which is in excellent agreement with the observed value of 331.1 nm. More importantly, the calculated near-field intensity pattern of this mode [Fig. 2(d), inset] approximates the observed image of the collimated fiber ultraviolet output on a white (fluorescent) paper [Fig. 2(a), inset]. Thus, the observed 331.1-nm line propagates in the 32nd mode of the fiber. The mode predicted at 327.6 nm has the closest pattern [Fig. 2(c)], and can be linked to the weak THG line that accompanies the dominant THG line [Fig. 1(d), blue arrow]. Note that these two modes, unlike other neighboring phase-matched modes with their distinct patterns [Fig. 2(c)], have no analogs in a conventional circular fiber.

Interestingly, the dominant THG lines of other fibers exhibit the same spatial pattern [Fig. 2(a), inset], indicating that the same intermodal THG is stimulated. By fixing the phase-matched signal mode to be the 32nd mode, the mode solver is used to calculate the wavelengths of these lines [Fig. 2(d)]. Despite the simple model (Fig. 1, inset A) with no adjustable parameter, the calculated wavelength approximates the observed value for each fiber (Table II). Thus, the THG emits at a wavelength strictly defined by the dielectric structure of fiber cross section. We note that prior studies supporting the static view [1,12] have predicted the wavelengths of different intermodal THGs for a given fiber. In contrast, the simulations and experiments in this study predict the variation of the wavelength of a given intermodal THG in a series of fibers, and unambiguously reveal the fiber effect on the THG wavelength (Table II). Alternative interpretations of this fiber effect from the dynamic view do not seem plausible.

The static view can be further appreciated by the use of a simple analogy. The emergence of sharp fiber THG lines from the excitation ultrafast fiber continuum in the momentum (β) domain [Figs. 1(a)–1(g), except Fig. 1(c)] is analogous to that of atomic absorption lines from a thermal irradiation continuum in the energy (frequency υ) domain, in the sense that the line positions are independent of the spectral shapes of the incident continua. It should be noted that β of the ultrafast fiber continuum and υ of the thermal irradiation continuum at a specific wavelength λ are fully determined by $\beta = 2\pi n_{\text{eff}}/\lambda$ and $\upsilon = c/\lambda$, respectively. The emission (positive) signal of the former is a resonant response of the fiber to a narrow-band component of the ultrafast continuum, just like the absorption (negative) signal of the latter is a resonant response of the atoms to that of the thermal irradiation continuum (Table III). The dominance of the 32nd mode over its neighboring modes [compare Figs. 1(d), 1(e), and 2(c), arrows] can be understood through the selection rule that governs the transition probability of atomic absorption (Table III) [15]. The dominance of the same intermodal THG in similarly structured fibers is then not surprising because they are subjected to the selection-rule-like restriction of fiber NL-2.3-790.

Prior studies supporting the static view [1,12] did not justify why the THG could be either a line emission spectrally narrower than the frequency-tripled pump spectrum [signal spectral narrowing, Fig. 1(c)], or a broadband emission with bandwidth comparable to this spectrum [12]. This inconsistency might have motivated the interpretation of the signal spectral narrowing from the dynamic view [3]. However, this effect has a simpler interpretation from the static view, as shown below. It should be noted that the reliably measured bandwidth (FWHM) of a continuum-stimulated THG [Figs. 1(a) or 1(b)] is an asymptotic value attained at sufficient signal intensity (>1 μW), so that this value approximates that of the pump-stimulated THG [Fig. 1(c)] (Fig. 1, inset B). Otherwise, a larger bandwidth is attained at lower signal intensities [compare the 353.4-nm lines in Figs. 1(f) and 1(g)]. This is because the continuum-stimulated THG occurs in a short interaction length L at the end of the fiber, leading to a large phase-matched bandwidth [Fig. 1(g)] according to the factor $\text{sinc}^2(\Delta\beta L/2)$ in Table III. Thus, the elongated L at a higher coupling power (or signal intensity) results in a narrower phase-matched bandwidth [Fig. 1(f)]. When L approaches the walk-off length between the fundamental and THG pulses, a condition termed as saturated phase matching, the bandwidth reaches the asymptotic value. The pump-stimulated THG, however, is generated immediately at the fiber entrance, so that the saturated phase-matching condition is automatically satisfied, and the bandwidth is independent on the coupling power or signal intensity [Fig. 2(b), inset].

Under the saturated phase-matching condition in a given fiber, the asymptotic bandwidth of the dominant THG line can be reliably measured (Table II). The bandwidth is inversely correlated to the differential slope of the two effective index curves at the corresponding intersection point [Fig. 2(d)] (Table II). Or more intuitively, the phase-matched bandwidth is inversely proportional to the angle of the intersection. This correlation explains why a prior study [12] supporting the static view did not produce line-shaped THG. In that study, due to the small differential slope at the intersections ($\sim 1.0 \times 10^{-4}$ nm^{-1}), the phase-matched bandwidth is estimated to be as broad as 2 nm, in good agreement with the observed value of

TABLE III. Continuum-excited fiber THG and atomic absorption.

Analog	Fiber THG	Atomic absorption
Stationary state	Fiber mode field	Atomic wave function
Discrete variable	β: Propagation constant for momentum state	ν: Frequency for energy state
Conjugate variable	L: Fiber length	T: Time
Resonance	Phase matching: $\Delta\beta = \beta^h(\omega_h) - 3\beta(\omega_h/3) = 0$	Bohr condition: $\Delta\nu = \nu_2 - \nu_1 - \nu_{\text{photon}} = 0$
Nature of spectral line signal	Positive, classical, nonlinear	Negative, quantum mechanical, linear
Background	Ultrafast fiber continuum in momentum domain	Thermal continuum in energy domain
Transition probability	$\propto$ Mode overlap, $\propto L^2\text{sinc}^2(\Delta\beta L/2)$[a]	$\propto$ Transition dipole, $\propto T^2\text{sinc}^2(\Delta\nu T/2)$[b]

[a]Reference [5].
[b]Reference [15].

~3 nm [12]. Thus, both the wavelength and the (asymptotic) bandwidth of the THG are intrinsic properties of the fiber. The variation of the bandwidth of a given intermodal THG in a series of fibers definitely reveals another fiber effect on the THG (Table II), in consistency with the static view. The broad asymmetric THG spectra observed in Ref. [8] may be complicated by imperfect fiber tapering [16], and are not solid evidence to support the dynamic view and reject the static view.

The three new pieces of evidence of fiber THG under continuum generation in this study, including the accurate localization of the fundamental, the absence of Kerr effect or pump dependence before fiber optical damage, and the fiber effect on the wavelength and bandwidth of a given intermodal THG, are sufficient to disprove the conventional dynamic view of fiber THG in favor of the static view. Why does the dynamic view succeed in fiber FWM but fail in fiber THG? We note that the role of the anharmonic shift Ω in the THG is different from that of the Stokes shift Ω_s in the FWM (Table I). The FWM counterpart of Ω should be $\Omega' = (\omega_s + \omega_{as} - 2\omega_p)$, where ω_s and ω_{as} are the Stokes frequency and anti-Stokes frequency, respectively. Unlike Ω_s ($\Omega_s = \omega_p - \omega_s$), the introduction of a nonzero Ω' into FWM phase-matching conditions would demand different detuning from ω_p for Stokes and anti-Stokes signals, which in quantum optics is forbidden by the law of conservation of photon energy, and has therefore never been observed. It is then reasonable to assume that the very concept of Ω (i.e., anharmonic THG) violates the law of photon energy conservation. As a result, the general theory of fiber THG should be modified to eliminate Ω in the derived phase-matched conditions (Table I), and by doing so, should ultimately recover the static view. On the other hand, this law forbids the THG counterpart of variable Ω_s, which may be responsible for the absence of the dynamic view of fiber THG. We believe that the static view may also hold in fiber intermodal second-harmonic generation (SHG), and the anharmonic effect should also be reevaluated in the corresponding SHG theory [5].

This research was supported in part by grants from the National Science Foundation (Grant No. CBET 10-33906) and the National Institutes of Health (Grants No. R01 EB013723 and No. R01 CA166309).

[1] L. Tartara, I. Cristiani, V. Degiorgio, F. Carbone, D. Faccio, M. Romagnoli, and W. Belardi, Opt. Commun. **215**, 191 (2003).
[2] S. O. Konorov, A. A. Ivanov, M. V. Alfimov, and A. M. Zheltikov, Appl. Phys. B **81**, 219 (2005).
[3] A. M. Zheltikov, Phys. Rev. A **72**, 043812 (2005).
[4] V. Grubsky and A. Savchenko, Opt. Express **13**, 6798 (2005).
[5] G. P. Agrawal, *Nonlinear Fiber Optics* (Academic Press, New York, 2007), Chaps. 10 and 12.
[6] J. D. Harvey, R. Leonhardt, S. Coen, G. K. L. Wong, J. C. Knight, W. J. Wadsworth, and P. St. J.Russell, Opt. Lett. **28**, 2225 (2003).
[7] A. Y. H. Chen, G. K. L. Wong, S. G. Murdoch, R. Leonhardt, J. D. Harvey, J. C. Knight, W. J. Wadsworth, and P. St. J. Russell, Opt. Lett. **30**, 762 (2005).
[8] D. A. Akimov, A. A. Ivanov, A. N. Naumov, O. A. Kolevatova, M. V. Alfimov, T. A. Birks, W. J. Wadsworth, P. St. J. Russell, A. A. Podshivalov, and A. M. Zheltikov, Appl. Phys. B **76**, 515 (2003).
[9] E. E. Serebryannikov, A. B. Fedotov, A. M. Zheltikov, A. A. Ivanov, M. V. Alfimov, V. I. Beloglazov, N. B. Skibina, D. V. Skryabin, A. V. Yulin, and J. C. Knight, J. Opt. Soc. Am. B **23**, 1975 (2006).
[10] A. B. Fedotov, A. A. Voronin, E. E. Serebryannikov, I. V. Fedotov, A. V. Mitrofanov, A. A. Ivanov, D. A. Sidorov-Biryukov, and A. M. Zheltikov, Phys. Rev. E **75**, 016614 (2007).
[11] K. Bencheikh, S. Richard, G. Mélin, G. Krabshuis, F. Gooijer, and J. A. Levenson, Opt. Lett. **37**, 289 (2012).
[12] A. Efimov, A. J. Taylor, F. G. Omenetto, J. C. Knight, W. J. Wadsworth, and P. St. J. Russell, Opt. Express **11**, 2567 (2003).
[13] A. A. Ivanov, D. Lorenc, I. Bugar, F. Uherek, E. E. Serebryannikov, S. O. Konorov, M. V. Alfimov, D. Chorvat, and A. M. Zheltikov, Phys. Rev. E **73**, 016610 (2006).
[14] Y. Vidne and M. Rosenbluh, Opt. Express **13**, 9721 (2005).
[15] D. A. Mcquarrie and J. D. Simon, *Physical Chemistry* (University Science Books, Sausalito, CA, 1997), Chap. 13.
[16] T. Lee, Y. Jung, C. A. Codemard, M. Ding, N. G. R. Broderick, and G. Brambilla, Opt. Express **20**, 8503 (2012).